Piezo Ink Jet Simulations Using the Finite Difference Level Set Method and Equivalent Circuit

Jiun-Der Yu, Epson Palo Alto Laboratory, Palo Alto, California

Shinri Sakai, Seiko Epson Corporation, Shiojiri, Nagano, Japan

Abstract

We developed a finite difference ink jet simulation code based on the coupled level set projection method on nonrectangular grids. A slipping contact model was applied to resolve the contradiction of the moving contact point and the no-slip condition. For practical applications, the code was connected to an equivalent circuit which receives a dynamic voltage and simulates the ink behavior in the supply channel under the influence of ink cartridge, vibration plate, and PZT actuator. Simulation results of continuous droplet ejections are given and discussed.

1. Introduction

Piezoelectric drop-on-demand ink jet print heads require a long development cycle to meet design goals. To speed up the process, numerical simulation of the ink jets can be used. Fig. 1 shows how a practical ink-jet simulation may be carried out. An equivalent circuit receives as an input the dynamic voltage to be applied to the piezoelectric PZT actuator and simulates the ink behavior under the influence of the ink cartridge, supply channel, vibration plate, and PZT actuator. It calculates an inflow pressure to drive the simulation code. The simulation code then solves the incompressible Navier-Stokes equations for two-phase flows for fluid velocity, pressure and interface position, and feeds back the ink flow rate to the equivalent circuit. The sequence is repeated as long as needed.

Since the print head nozzle geometry can be very complicated, the traditional rectangular grid of finite difference method usually results in the staircase pattern at solid boundaries that are not parallel to the coordinate axes. To solve the problem, we recently developed a finite difference simulation code based on the coupled level set projection method on quadrilateral grids. The level set method was applied to capture the ink-air interface. The projection scheme was adopted to enforce the incompressibility. A slipping contact line model was used to resolve the contradiction of the moving contact point and the no-slip condition.

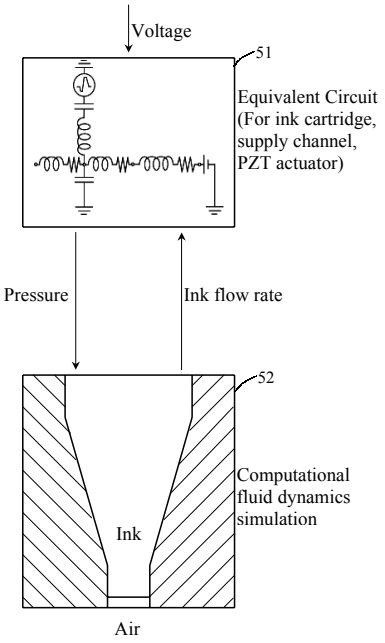

Figure 1. The connection between the CFD code and equivalent circuit for ink jet simulations.

In this paper, the detail of the special finite difference method and its connection with the equivalent circuit will be presented. A simulation example will be given and discussed.

2. Governing Equations

The governing equations for two-phase (ink and air) flows consist of the continuity equation

$$\nabla \cdot u = 0, \tag{1}$$

and the Navier-Stokes equations

$$\frac{D\boldsymbol{u}}{Dt} = -\frac{\nabla p}{\rho(\phi)} + \frac{\nabla \cdot (2\mu(\phi)\mathcal{D})}{\rho(\phi)Re} - \frac{\kappa(\phi)\delta(\phi)\nabla\phi}{\rho(\phi)We}. \tag{2}$$

In the above equations, $\mathcal{D} = 1/2\,[\nabla u + (\nabla u)^T]$ is the rate of deformation tensor, $u = ue_1 + ve_2$ is the fluid velocity, $D/Dt = \partial/\partial t + (u \cdot \nabla)$ is the Lagrangian time derivative, p the pressure, δ the Dirac delta function, κ the curvature, ϕ the level set. The density ratio, viscosity ratio, Reynolds number, and Weber number are defined by

$$\rho(\phi) = \begin{cases} 1 & \text{if } \phi \geq 0 \\ \rho_2/\rho_1 & \text{if } \phi < 0 \end{cases}, \quad Re = \frac{\rho_1 U L}{\mu_1}, \\ \mu(\phi) = \begin{cases} 1 & \text{if } \phi \geq 0 \\ \mu_2/\mu_1 & \text{if } \phi < 0 \end{cases}, \quad We = \frac{\rho_1 U^2 L}{\sigma}, \tag{3}$$

where σ is the surface tension coefficient, ρ_i the density of the ith fluid, μ_i the dynamic viscosity of the ith fluid, U the velocity scale, and L the length scale.

We use the level set method[1] to capture the ink-air interface, and hence the density, dynamic viscosity, and curvature are all defined in terms of the level set ϕ, given by

$$\phi(x,y,t) \begin{cases} < 0 & \text{if} \quad (x,y) \in \text{fluid 2 (air)} \\ = 0 & \text{if} \quad (x,y) \in \text{interface} \\ > 0 & \text{if} \quad (x,y) \in \text{fluid 1 (ink)} \end{cases}. \tag{4}$$

The level set function ϕ is initialized as the signed distance to the interface. The curvature of the interface can be obtained by $\kappa = \nabla \cdot (\frac{\nabla\phi}{|\nabla\phi|})|_{\phi=0}$. Since the interface moves with the fluid, the evolution of the level set is governed by

$$\frac{\partial \phi}{\partial t} + \boldsymbol{u} \cdot \nabla \phi = 0\,. \tag{5}$$

3. Numerical Algorithm

3.1. Time Integration

Suppose we know quantities u^n, p^n, ϕ^n, the purpose of an algorithm is to obtain u^{n+1}, p^{n+1}, ϕ^{n+1}. The following algorithm is first-order accurate in time.

3.1.1. Level Set Update

The level set is updated first by

$$\phi^{n+1} = \phi^n - \Delta t\,[\boldsymbol{u} \cdot \nabla \phi]^{n+1/2} \tag{6}$$

The second-order explicit Godunov scheme[2] is applied for the time-centered advection term $[u \cdot \nabla\phi]^{n+1/2}$. Once ϕ^{n+1} is obtained, we compute $\phi^{n+1/2}$ by

$$\phi^{n+1/2} = \frac{1}{2}\left(\phi^n + \phi^{n+1}\right). \tag{7}$$

3.1.2. Explicit Euler for Navier-Stokes Equations

Let the velocity predictor be

$$\boldsymbol{u}^* = \Delta t \left\{ \frac{\nabla \cdot [2\mu(\phi^{n+1/2})\mathcal{D}^n]}{\rho(\phi^{n+1/2})Re} - [(\boldsymbol{u} \cdot \nabla)\boldsymbol{u}]^{n+1/2} - \frac{[\kappa(\phi)\delta(\phi)\nabla\phi]^{n+1/2}}{\rho(\phi^{n+1/2})We} \right\} + \boldsymbol{u}^n, \tag{8}$$

the time-discretized Navier-Stokes equations can be written as

$$\boldsymbol{u}^{n+1} = \boldsymbol{u}^* - \frac{\Delta t}{\rho(\phi^{n+1/2})}\nabla p^{n+1}. \tag{9}$$

We apply the second-order explicit Godunov scheme[2] for the advection term and the central difference for the viscosity and surface tension terms in (8). It is noted that the determination of u^* needs only values at time step n.

3.1.3. Projection for u^{n+1}

To satisfy the incompressibility condition for time step n+1, we apply the divergence operator on both sides of (9). Since $\nabla \cdot u^{n+1} = 0$, we have

$$\nabla \cdot \boldsymbol{u}^* = \nabla \cdot \left(\frac{\Delta t}{\rho(\phi^{n+1/2})} \nabla p^{n+1} \right). \tag{10}$$

After the pressure p^{n+1} is solved from equation (10), the velocity field u^{n+1} can be obtained by (9).

3.2. Quadrilateral Grid

A body-fitted quadrilateral grid as shown by the first figure of Fig. 2 is used for the ink jet simulation. The difficulty of using a non-rectangular grid with a finite difference method is the calculation of the space derivatives. In our work, we assume there exists a transformation $X = \Phi(\Xi)$ which maps the uniform square grids in a computational space $\Xi = (\xi, \eta)$ (see the second figure in Fig. 2, $\Delta\xi = \Delta\eta = 1$) to the quadrilateral grids in the physical space $X = (r, z)$. The Jacobian and the transformation matrix are defined to be

$$J = g \det \nabla_\Xi \Phi = g \det \begin{pmatrix} r_\xi & r_\eta \\ z_\xi & z_\eta \end{pmatrix}, \\ \boldsymbol{T} = g^{-1} J\,[\nabla_\Xi \Phi]^{-1} = \begin{pmatrix} z_\eta & -r_\eta \\ -z_\xi & r_\xi \end{pmatrix}, \tag{11}$$

where $g = 2\pi r$ in the axi-symmetric coordinate system. It is not necessary to construct the global mapping Φ. Only the local Jacobian and transformation matrix are calculated. Differences of the quadrilateral grid points in the physical space are used to define the elements of the transformation matrix and the Jacobian at cell centers, i.e.,

$$(X_\xi)_{i,j} = \frac{1}{2}\left(X_{i,j} - X_{i-1,j} + X_{i,j-1} - X_{i-1,j-1}\right). \tag{12}$$

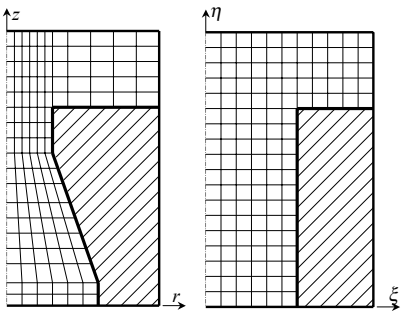

Figure 2. The quadrilateral grid in physical space and the uniform square grid in computational space.

Since the numerical differentiation in the computational space is easy, space derivatives are calculated there and then transferred to the physical space. For example,

$$\begin{aligned} \nabla p &= \begin{pmatrix} p_r \\ p_z \end{pmatrix} = \begin{pmatrix} \xi_r & \eta_r \\ \xi_z & \eta_z \end{pmatrix} \begin{pmatrix} p_\xi \\ p_\eta \end{pmatrix} \\ &= gJ^{-1} \begin{pmatrix} z_\eta & -z_\xi \\ -r_\eta & r_\xi \end{pmatrix} \begin{pmatrix} p_\xi \\ p_\eta \end{pmatrix} \\ &= gJ^{-1}\boldsymbol{T}^T \nabla_\Xi p \,. \end{aligned} \tag{13}$$

3.3. Contact Model

Because the no-slip condition for viscous fluid at solid boundaries contradicts the fact that the contact point keeps sliding on the nozzle wall in ink jet simulations, we need a contact model to solve the problem. We first define the contact angle θ as the angle made by the ink-air interface and the solid, measured from the side of ink by approaching the contact point as close as possible. The advancing critical contact angle θ_a and receding critical contact angle θ_r are the maximum and minimum contact angles for the contact point to stay. In most situations $\theta_r < \theta_a$. Actual values of θ_a and θ_r depend on both the fluids and the solid surface. We use the following criteria to decide whether to let the triple point move: (1) The triple point is allowed to move toward the air side if $\theta \geq \theta_a$; The triple point is allowed to move toward the ink side if $\theta \leq \theta_r$; (3) The triple point should not move otherwise. If the triple point is not allowed to move, the boundary condition at the solid wall is the no-slip condition. If the triple point is allowed to move, the no-slip condition in a close vicinity of the triple point is switched to the free slip condition. In this work, we chose to set two cells at each side of the contact point to free slip should the triple point be allowed to move.

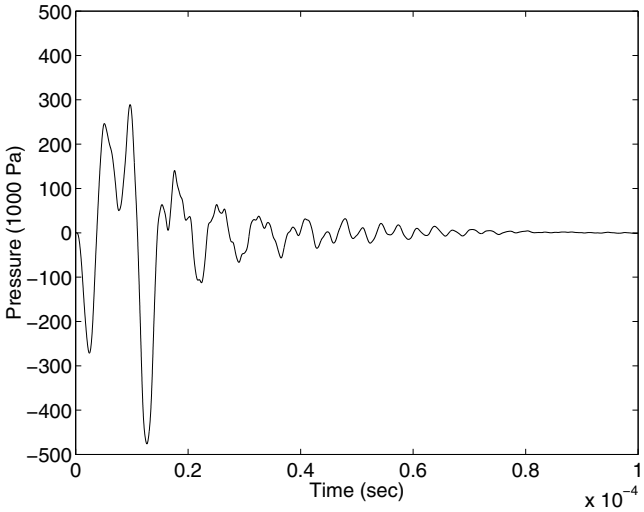

Figure 3. The typical inflow pressure.

3.4. Equivalent Circuit

In a piezo ink jet print head, the formation of ink droplets is controlled by a piece of piezoelectric PZT actuator. Driven by the input voltage, the PZT would push and pull the ink. For numerical simulation of ink jet, one needs to prescribe a velocity or pressure at the nozzle inflow. However, only the input voltage to the PZT is known. An equivalent circuit model can be used to solve the problem. The ink flow rate and pressure are first taken as dependent variables. Each component of the ink jet print head, such as the nozzle, pressure chamber, vibration plate, PZT actuator, and ink cartridge, is expressed in terms of the compliance and acoustic resistance. These acoustics elements are finally transferred to their equivalent inductance, capacitance, and electric resistance to form an equivalent circuit. By solving the equivalent circuit and the flow equations in turn, one simulates a real ink jet.

The particular equivalent circuit we used is not described here; readers are referred to Sakai[3] for an introduction to print head structures and equivalent circuits. A typical inflow pressure is shown in Figure 3. The driving voltage is such that the ink is first pulled back, pushed and fired, and pulled back to get ready for the next ejection. The pressure pattern contains a high frequency signal. It is basically the fundamental natural frequency of the system, which is several times higher than the driving voltage frequency in this case.

4. Numerical Example

As an example of ink jet simulation, we consider a nozzle of diameter 26 microns at the opening and 52.0 microns at the bottom. The length of the nozzle opening part, where the diameter is 26 microns, is 25 microns. The shrinking part of the nozzle is 55 microns and the bottom part is 7.8 microns. The inflow pressure is as shown in Figure 3 and is repeated at a frequency of about 10*KHz*. The solution domain was chosen to be $\{(r, z)|0 \leq r \leq 32.5\mu m,\ 0 \leq z \leq 390\ \mu m\}$. The advancing and receding critical contact angles are 70° and 20°, respectively. The initial meniscus is assumed to be flat with the nozzle opening. For the purpose of normalization, we chose the nozzle opening diameter (26 microns) to be the length scale and 6 *m/sec* to be the velocity scale. The normalized solution domain is hence $\{(r, z)|0 \leq r \leq 1.25,\ 0 \leq z \leq 15.\}$. Since the density, viscosity, and surface tension of ink are approximately $\rho_1 = 1070$ *Kg/m*^{3}, $\mu_1 = 3.5 \times 10^{-3}$ *Kg/m· sec*, $\sigma = 0.032$ *Kg/sec*^{2}, the Reynolds number and Weber number are *Re* = 47.7, *We* = 31.3.

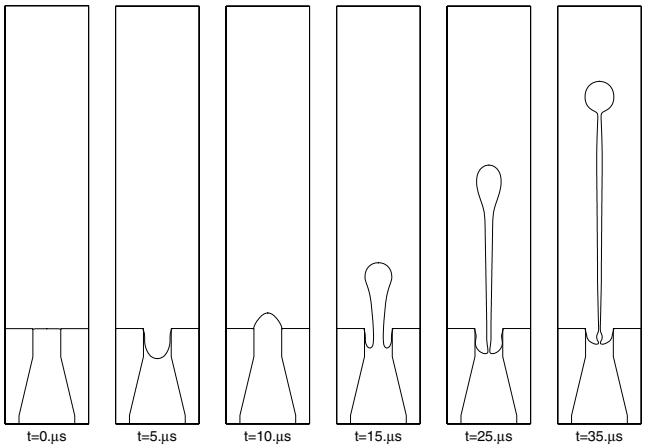

Figure 4. The ejection of the first droplet.

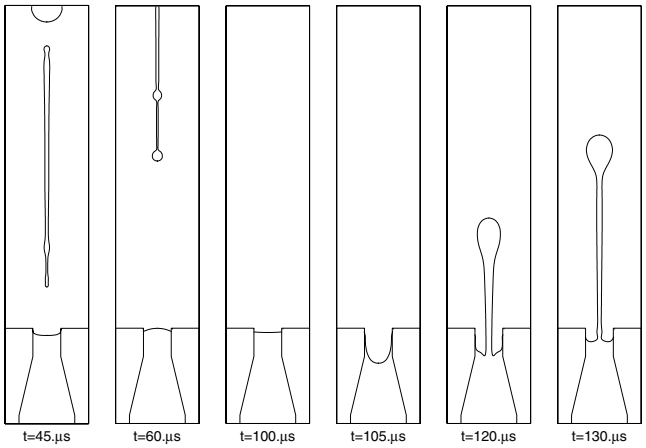

Figure 5. The ejection of the second droplet.

Simulation results of continuous droplet ejection are plotted in Fig. 4 and 5. We see from Fig. 4 that the first droplet pinches off in the nozzle at t = 35.0 μs. The long droplet continues moving forward and breaks into a major droplet and one or more satellites. The meniscus is concave at t = 35.0 μs. The capillary force helps pull the ink in the nozzle upward so that the ink flows from the cartridge into the nozzle. The meniscus returns to the nozzle exit and recovers to almost a straight line at t = 100.μs before the nozzle is ready for the next ejection. The second droplet as shown in Fig. 5 is almost of the same size as the first one. The average droplet size from the simulation is 13 pico liters, which is very close to the experimental observation.

As a conclusion, we developed a finite difference ink jet simulation code based on the coupled level set projection method on quadrilateral grids. A slipping contact model was applied to resolve the contradiction of the moving contact point and the no-slip condition. The code was connected to an equivalent circuit for practical simulations. The droplet shape, size, and pinch off time are in good agreement with experimental observations.

References

1. Osher, S. & Sethian, J.A., Fronts Propagating with Curvature-Dependent Speed: Algorithms Based on Hamilton–Jacobi Formulations, J. of Comp. Physics, 79, pp. 12-49, 1988.
2. John B. Bell and Phillip Colella, "A Projection Method for Viscous Incompressible Flow on Quadrilateral Grids," AIAA Journal, 32(10), 1961 1994.
3. Sakai, S. Dynamics of Piezoelectric Inkjet Printing Systems. Proc. IS&T NIP 16, (2000) 15-20.

Biographies

Jiun-Der Yu got his PhD from Princeton University in 1995. He is currently the manager of the Device Modeling group of Palo Alto Laboratory, Epson Research and Development, Inc. Piezo-electro-magnetism, wave propagation, and computational fluid dynamics are his major research interests.

Shinri Sakai is a chief specialist in the Printer Development Division of Seiko Epson Corporation. He received his B.E. and M.E. in mechanical engineering from Tokyo Institute of Technology, Japan, in 1983 and 1985 respectively. His primary responsibilities are mechanical and physical analysis and computer simulation for ink jet head development and optimization. His recent interests are rheological features of inks and their contribution to ink meniscus and droplet formation.